Model of phonon excitation by fast electrons in a crystal with correlated atomic motion

A. V. Martin, S. D. Findlay, and L. J. Allen
School of Physics, University of Melbourne, Victoria 3010, Australia
(Received 31 March 2009; revised manuscript received 1 July 2009; published 27 July 2009)

When fast electrons are used to study matter at subnanometer length scales, it is often necessary to model the inelastic cross section and the absorptive effect of phonon excitation on elastically scattered electrons. The inelastic cross section for the excitation of a phonon in a crystal by a fast electron is well modeled by using an effective absorptive potential. In this paper, the absorption potential for phonon excitation by fast electrons is rigorously derived from many-body quantum mechanics taking into account correlated atomic motion. This potential is calculated for a silicon crystal at room temperature from the force constants and dispersion curves for the crystal. It is shown that the *total* absorption for a crystal at room temperature predicted by a phonon model with correlated atomic motion agrees with the Einstein-model potential, based on independent atomic motions. This suggests that ignoring correlated atomic motion is not likely to contribute to the well-known quantitative discrepancy in contrast between simulated and experimental transmission electron microscopy images (the so-called "Stobbs factor"). The quantum-mechanical formulation allows us to further investigate the form of the inelastically scattered waves and the nonlocality of the absorption potential in directions both perpendicular and parallel to the direction of propagation, providing deeper insight into underlying physics of phonon excitation by fast electrons.

DOI: 10.1103/PhysRevB.80.024308 PACS number(s): 63.20.kd, 61.05.jd

I. INTRODUCTION

The excitation of phonons by fast electrons has been a topic of considerable interest for over fifty years[1–7] and continues as a highly active area of research because of its importance to electron microscopy.[8–15] Electrons can be focused into areas less than a square angstrom and interact strongly with matter, making them ideal for studying nanostructures on the atomic scale. However, this strong interaction means that both multiple elastic and inelastic-scattering events contribute to measurements of even the thinnest samples.[16] The theory that describes these scattering processes is well known[17] but in practice calculations are difficult to implement. The problem of elastic scattering to all orders was solved with the Bloch wave[18] and multislice methods.[19] However, incorporating inelastic scattering by phonon excitation,[1–7,13,14] plasmon excitation,[20] or the ionization of an atom[18,21] requires more complex models. The development and improvement of these models is ongoing.

Early interest in phonon excitation was driven by the observed effects on electron-diffraction patterns. Phonon excitation leads to attenuation of the wave function describing elastic scattering,[4,16] causing attenuation of the intensities of Bragg peaks in a diffraction pattern. Thermally scattered electrons produce a diffuse background in diffraction patterns, which contains features such as Kikuchi lines.[22]

Phonon excitation has come under renewed scrutiny in the push toward quantitative atomic resolution electron microscopy. In transmission electron microscopy (TEM), for instance, there is still a discrepancy between the contrast of experimental TEM images and simulations, and the cause remains unknown.[23] This is commonly known as the Stobbs factor. Predicting TEM images requires an accurate knowledge of the elastic wave function, which is sensitive to the levels of absorption in the crystal.[16] Hence, phonon excitation must be modeled to accurately simulate and interpret these images.[3] A deficiency in the understanding of phonon scattering is one of several theoretical issues that may potentially contribute to the discrepancy.[24] For example, it has been speculated that an underestimate of the amount of thermal scattering could contribute to the mismatch factor.[23] This has led to attempts to quantify the amount of phonon scattering in TEM (Ref. 11) and to determine the coherence of these inelastically scattered waves.[12] Checking the adequacy of thermal scattering models used in TEM simulation was a key motivation for the work presented here.

Electrons that have excited phonons in a crystal can be measured directly with a high-angle annular dark-field (HAADF) detector in scanning transmission electron microscopy (STEM). The signal is sensitive to atomic number and allows for identification of atomic species within a column.[25] Recently, the first quantitative comparison between theory and experiment for a HAADF STEM experiment at atomic resolution has been achieved.[15] A comprehensive understanding of phonon scattering provides a solid foundation for quantitative STEM, which hopefully will become routine.

Two distinct approaches have been developed to calculate the influence of thermal scattering on TEM and STEM experiments: a model based on an imaginary absorptive potential and the frozen-phonon model. An imaginary potential, inserted into the time-independent wave equation for the fast electron, describes the attenuation of the elastic beam. It can also be used to calculate the amount of thermally scattered signal collected by a HAADF detector. The inclusion of an imaginary potential is rigorously justified from time-independent quantum mechanics, for instance the coupled-channel approach of Yoshioka.[17] In contrast, the frozen-phonon model is motivated by the understanding that the time taken for the electron to traverse the crystal is much faster than the thermal oscillations of an atom.[19] The electron wave function is calculated for a particular displacement of atoms, and a measurement is built up by a weighted incoherent sum over different configurations of atomic displace-

 ©2009 The American Physical Society

ments. An intuitive interpretation of the frozen-phonon model would suggest that it predicts elastic scattering from a crystal with a finite temperature. This is a different physical picture from that which underlies the quantum-mechanical (QM) absorptive model, which is based explicitly on phonon excitation. Both models have been shown to agree with one another and with experiment,[15] provided the single inelastic-scattering approximation is valid (which is used to implement the absorptive model). Hence, we believe that both approaches will continue to make important contributions to the understanding and prediction of thermal scattering. Recently, progress has been made on understanding the agreement between the two models using analytic arguments.[26]

Irrespective of the method chosen to solve the wave equation for the fast electron in the crystal, a choice must be made about how the vibrations of the crystal are to be modeled. The most common model used in calculations for electron microscopy is the Einstein model, which assumes that each atom vibrates independently. The imaginary potential in the Einstein model has been known for some time and can be derived using either semiclassical[1] or quantum-mechanical formulations.[2,13] It became a standard part of calculations when the computational resources became available.[4] It is usually assumed that the vibrations are isotropic, in which case the absorption potential is parametrized by a single Debye-Waller factor. Anisotropic vibrations can be included[9] and, for example, have a significant effect on the absorptive potential for aluminum.[13] Similarly, the frozen-phonon model is most commonly implemented with the Einstein model, assuming each atom vibrates independently. The Einstein model was assumed in the recent investigation of the agreement between the absorptive and frozen-phonon models.[26]

In reality, the thermal motion of the atoms in a crystal is a collective motion. The motion between atoms is correlated and the excitations of this collective motion are known as phonons. In the literature for fast electron scattering, sometimes the term "phonon excitation" is used, even when independent atomic vibrations are assumed in the calculation. We would like to clarify that we will only use the word phonon to denote a collective vibration of atoms, with the exception of the term "frozen-phonon model," which we inherit from the literature. Vibrational modes are described with the Born-von Karman model of lattice dynamics and are characterized by the dispersion curves and force constants of a crystal. It is known that correlated atomic motion is responsible for structure in the diffuse background of a diffraction pattern.[7] However, existing calculations of thermal scattering with correlated atom vibrations have not utilized all the phonon information but require additional levels of approximation, which can be quite severe. For example, calculations have been limited to a few Bloch waves,[2,27] systematic row conditions,[27] or the Debye model.[2,7] There is one notable exception: a comprehensive treatment of correlated atomic motion was included in a frozen-phonon calculation, which predicted banded features in convergent-beam electron diffraction (CBED) patterns that were also observed in experiment, but which are not predicted by the Einstein model.[14] However, since the frozen-phonon model is semiclassical, it remains to be seen how the correlated atomic vibrations affect the absorption potential within a fully quantum-mechanical model of thermal scattering.

In this paper, we provide a derivation of the absorption potential due to phonon excitation from within the framework of many-body quantum mechanics. The derivation is based on the Born-von Karman theory of lattice dynamics,[28] which includes anisotropy in the potential. The form of the absorptive potential for phonon excitation used in the quantum-mechanical formulation is known[7,29] but has not been evaluated because of its complexity. Using our derived expression, absorption potentials are calculated for a silicon crystal at room temperature, starting with the force constants and phonon-dispersion curves. This calculation is an advance on what was previously achieved for calculations of an absorption potential with collective atomic vibration. This quantum-mechanical model including correlated atomic motion is referred to in this paper as the "QM-phonon model." The total absorption predicted by the QM-phonon model agrees with that predicted by the Einstein-model potential. This suggests that neglecting correlated atomic motion in thermal scattering models is not likely to contribute to the Stobbs factor.

The inelastically scattered waves generated by the excitation of a phonon and those predicted by the Einstein model differ significantly. In the phonon case, a single inelastic wave can take a contribution from every atom in the crystal, whereas in the Einstein model each inelastic wave only takes a contribution from a single atom. This is important because ultimately the propagation of such waves determines where the inelastic scattered electrons are in the diffraction pattern, causing structure in the diffuse background. Recently, the ionization of an atom in a crystal by a fast electron has been successfully modeled by the explicit calculation and propagation of inelastic waves.[21,30] The form of the waves that describe electrons after exciting a phonon is derived and compared to those predicted by the Einstein model.

Electrons scattered to high angles are measured in STEM with annular detectors. Inelastically scattered electrons make a more significant contribution to the measured signal than elastically scattered electrons. The signal measured can be calculated using an effective absorption potential,[31] and if the angular range is small enough this potential is nonlocal in the plane perpendicular to propagation.[32] We calculate the effective nonlocal potential for a point detector predicted by the correlated phonon model and compare it to the Einstein model. It is shown that correlated atomic motion changes the nonlocal potential significantly. However, we do not expect these differences to be observed in STEM experiments since the angular range spanned by the detector is typically large enough to ensure the validity of the local approximation.

The nonlocality of the potential in the direction of propagation is not determined by the size of the detector and, because phonon excitations are delocalized, may be significant in this case. This issue has been explored previously[7] but it has not been checked by quantitative calculation of the nonlocal potential. Here we investigate this issue via calculation.

Electrons with low incident energies, i.e., 1–100 eV, can be used to perform phonon spectroscopy of surfaces in a reflection geometry.[33,34] The low incident energy used in

these methods means that the theory that models these experiments[35] is different from the theory presented in this paper for fast electron scattering.

II. ABSORPTION POTENTIAL

The coupled-channel approach of Yoshioka[17] describes the inelastic scattering of a fast electron incident on a crystal, starting with the many-body Schrödinger equation. When the single inelastic-scattering approximation is made in the Yoshioka formalism, the nonlocal absorptive potential is[32]

$$W(\mathbf{r},\mathbf{r}') = \frac{2\pi m}{h^2}\sum_{n\neq 0} H_{0n}(\mathbf{r})H_{n0}(\mathbf{r}')k_n \times \int e^{2\pi i\tilde{\mathbf{K}}\cdot(\mathbf{r}-\mathbf{r}')}\delta(k_n-\tilde{K})d\Omega_{\tilde{K}}d\tilde{K}, \quad (1)$$

where m is the relativistically corrected mass of the incident electron and $\mathbf{r}$ is a three-dimensional position vector, where k_n is the wave number of the scattered electron. The transition potentials are

$$H_{n0}(\mathbf{r}) = \langle a_n(\boldsymbol{\tau}_n,\boldsymbol{\tau}_e)|H'(\mathbf{r},\boldsymbol{\tau}_n,\boldsymbol{\tau}_e)|a_0(\boldsymbol{\tau}_n,\boldsymbol{\tau}_e)\rangle, \quad (2)$$

where $\boldsymbol{\tau}_n$ represents the set of all the atomic coordinates and $\boldsymbol{\tau}_e$ represents the set of all the electronic coordinates. The state vector $|a_0(\boldsymbol{\tau}_n,\boldsymbol{\tau}_e)\rangle$ represents the initial state of the crystal and $|a_n(\boldsymbol{\tau}_n,\boldsymbol{\tau}_e)\rangle$ represents the crystal in the nth excited state. We use the subscript 0 to denote the initial state although this does not necessarily mean the ground state of the crystal. The interaction term $H'(\mathbf{r},\boldsymbol{\tau}_n,\boldsymbol{\tau}_e)$ is given by

$$H'(\mathbf{r},\boldsymbol{\tau}_n,\boldsymbol{\tau}_e) = \sum_l H'_l(\mathbf{r},\boldsymbol{\tau}_n^l,\boldsymbol{\tau}_e^l) = \sum_l \left[\frac{Z_N e^2}{4\pi\epsilon_0|\mathbf{r}-\boldsymbol{\tau}_n^l|} - \sum_{i=1}^{N_l}\frac{e^2}{4\pi\epsilon_0|\mathbf{r}-\boldsymbol{\tau}_e^{l,i}|}\right], \quad (3)$$

where $\boldsymbol{\tau}_n^l$ denotes the atomic coordinates of the lth atom in the crystal, and $\boldsymbol{\tau}_e^{l,i}$ denotes the coordinates of the ith electron around the lth atom. In practice, the potential used in multislice calculations is projected in the direction of propagation (denoted by z) over the thickness of a unit cell. However, care must be taken when projecting the nonlocal potential. As indicated in Ref. 32, the wave equation that includes a projected nonlocal potential is only an accurate model if $W(\mathbf{r},\mathbf{r}')$ is only nonzero when z and z' belong to the same slice. This is not valid for phonon excitation because the interaction of potentials in different slices can contribute to the excitation of a single inelastic wave. Attempts to estimate the importance of this effect have been made.[7,36] However, the issue could be decisively resolved if $W(\mathbf{r},\mathbf{r}')$ could be calculated. A six-dimensional calculation of $W(\mathbf{r},\mathbf{r}')$ is not computationally feasible. For the moment, we will project the nonlocal potential and defer a discussion of the validity of the projection until Sec. IV, where the reduced quantity $W(\mathbf{r}_\perp=\mathbf{0},z,z')$ is calculated. We note that if coherence in the z direction cannot be ignored, there is a multislice-based scheme that can take this into account.[37]

We define the projected nonlocal potential as

$$W(\mathbf{r}_\perp,\mathbf{r}'_\perp) = \frac{1}{t}\int_0^t\int_0^t e^{-2\pi iKz}W(\mathbf{r},\mathbf{r}')e^{2\pi iKz'}dzdz', \quad (4)$$

where t is the thickness of the specimen in the z direction. The energy lost by a fast electron when it excites a phonon is typically of the order of meV so it is valid to approximate $k_n \approx K$, where K is the wave number of the incident electron. As shown in Appendix A, the Fourier coefficients of the projected nonlocal potential are given by

$$W(\mathbf{q}_\perp,\mathbf{q}'_\perp) = \frac{2\pi mK}{h^2 t_c}\sum_{n\neq 0}\int H_{0n}(\mathbf{q}_\perp-\tilde{\mathbf{K}}+K\hat{\mathbf{z}}) \times H_{n0}(\tilde{\mathbf{K}}-\mathbf{q}'_\perp-K\hat{\mathbf{z}})\delta(K-\tilde{K})d\Omega_{K'}d\tilde{K}, \quad (5)$$

where t_c is the thickness of a unit cell. In the local approximation, $W(\mathbf{q}_\perp,\mathbf{q}'_\perp)\approx W(\mathbf{q}_\perp-\mathbf{q}'_\perp)$.

In the Einstein model each atom is treated as an independent harmonic oscillator. In this case, we can write the many-body crystal wave function as the product of the harmonic-oscillator wave functions for individual atoms. Using this ansatz for the crystal wave function and making the local approximation, the absorption potential becomes[13]

$$W_{\mathbf{H}-\mathbf{G}} = \frac{Kh^2}{2\pi mV_c}\left[\sum_{l_u} e^{-2\pi i(\mathbf{H}-\mathbf{G})\cdot\mathbf{R}_{l_u}}\right]\int f_e(\mathbf{H}-\mathbf{G}-\mathbf{K}')f_e(\mathbf{K}') \times\{e^{-M_E(\mathbf{H}-\mathbf{G})^2} - e^{-M_E(\mathbf{H}-\mathbf{G}-\mathbf{K}')^2}e^{-M_E\mathbf{K}'^2} \times I_0[\tilde{M}|(\mathbf{H}-\mathbf{G}-\mathbf{K}')_x||\mathbf{K}'_x|]I_0[\tilde{M}|(\mathbf{H}-\mathbf{G}-\mathbf{K}')_y| \times|\mathbf{K}'_y|]I_0[\tilde{M}|(\mathbf{H}-\mathbf{G}-\mathbf{K}')_z||\mathbf{K}'_z|]\}d\Omega_{K'}, \quad (6)$$

where I_0 is a modified Bessel function and V_c is the volume of the unit cell. A Bloch wave expansion has been made, and $\mathbf{G}$ and $\mathbf{H}$ are vectors on the reciprocal lattice for the crystal. The sum over atoms l_u is restricted to atoms in the unit cell because the Bloch wave expansion has been made. We have also defined $\mathbf{K}'=\tilde{\mathbf{K}}-K\hat{\mathbf{z}}$. The Debye-Waller factor predicted by the Einstein model, M_E, is given by

$$M_E = \frac{\pi^2\hbar}{m_A\omega_0}\coth\left(\frac{\hbar\omega_0}{2k_BT}\right), \quad (7)$$

where ω_0 is the frequency of oscillation for a given atom, m_A denotes the mass of an atom (assuming a single atom type), k_B is Boltzmann's constant, and T is the temperature of the crystal. We have also defined

$$\tilde{M} = \frac{2\pi^2\hbar}{m_A\omega_0}\sinh^{-1}\left(\frac{\hbar\omega_0}{2k_BT}\right) = 2\sqrt{M_E^2-M_{T=0}^2}, \quad (8)$$

where $M_{T=0}$ is given by Eq. (7) calculated when $T=0$.

The form of the Fourier coefficients of the potential in Eq. (6) is similar to the standard form typically used in calculations,[4] with the exception of the modified Bessel functions, which appear because the potential has been thermally averaged with Bose-Einstein statistics. As shown in Fig. 1, the inclusion of the Bessel functions does not make a large difference to the absorption potential. In the limit that the

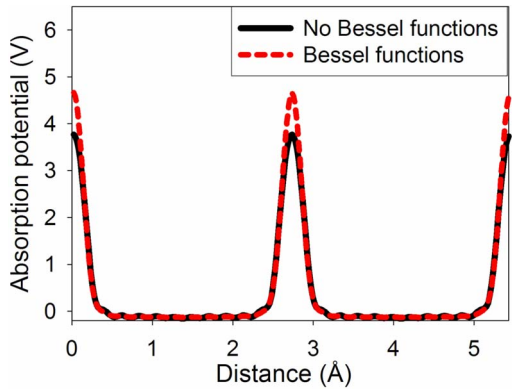

FIG. 1. (Color online) A line scan of the Einstein-model absorption potential in silicon at 293 K, viewed down the ⟨001⟩ zone axis. The potential was calculated using Eq. (6), with the Bessel functions, as predicted by the quantum-mechanical derivation, and without the Bessel functions, as predicted by the Hall and Hirsch model. Note that the potential and all subsequent figures are converted to volts (V) with a conversion factor of $h^2/(2me)$.

arguments of the Bessel functions approach zero, the values of the Bessel functions approach one, and in the other limit, as the arguments become large, the exponential terms in Eq. (6) tend to zero faster than the Bessel functions diverge. The potential in Eq. (6) has one parameter that characterizes the thermal properties of the crystal: the Debye-Waller factor. The Einstein-model theory is not used to calculate this parameter and its value is measured experimentally. The absorption potential can be generalized to include the anisotropic temperature-factor coefficients, which characterize anisotropy in the absorption potential.[9,38]

In Appendix B, it is shown that the nonlocal form of the Einstein-model potential is given by

$$W(\mathbf{q}_\perp,\mathbf{q}'_\perp)=\frac{Kh^2}{2\pi mV_c}\left[\sum_l e^{-2\pi i(\mathbf{q}_\perp-\mathbf{q}'_\perp)\cdot\mathbf{R}_l}\right]\int f_e(\mathbf{q}_\perp-\mathbf{K}')\times f_e(\mathbf{K}'-\mathbf{q}'_\perp)\{e^{-M_E(\mathbf{q}_\perp-\mathbf{q}'_\perp)^2}-e^{-M_E(\mathbf{q}_\perp-\mathbf{K}')^2}e^{-M_E(\mathbf{K}'-\mathbf{q}'_\perp)^2}I_0[\tilde{M}|(\mathbf{q}_\perp-\mathbf{K}')_x|\times|(\mathbf{K}'-\mathbf{q}'_\perp)_x|]I_0[\tilde{M}|(\mathbf{q}_\perp-\mathbf{K}')_y|\times|(\mathbf{K}'-\mathbf{q}'_\perp)_y|]I_0[\tilde{M}|(\mathbf{q}_\perp-\mathbf{K}')_z|\times|(\mathbf{K}'-\mathbf{q}'_\perp)_z|]\}d\Omega_{K'}. \quad (9)$$

In practice, it is rare to require the nonlocal form of the Einstein-model potential but we quote it here for use later in comparisons to the correlated vibration model.

The Debye-Waller factors have been calculated for elemental crystals and ionic compounds,[10] using the appropriate phonon-dispersion curves. The Debye-Waller factor is calculated using

$$M_P=\frac{\pi^2\hbar}{m_A}\int_0^{\omega_m}\coth\left(\frac{\hbar\omega}{2k_BT}\right)\left[\frac{g(\omega)}{\omega}\right]d\omega, \quad (10)$$

where ω is the angular frequency and $g(\omega)$ is the density of states obtained from phonon-dispersion curves. The Debye-Waller factors calculated with this formula are reasonably close to experiment.

What is still not clear, however, is whether the form of the potential given in Eq. (6) is adequate to describe absorption for correlated atomic motion. To derive the form of the potential consistent with phonon excitation we require the many-body wave functions that describe a crystal with correlated atomic motion. In the Born-von Karman model of lattice dynamics, a system of coupled harmonic oscillators is represented as a system of uncoupled normal modes.[28] Hence, if the crystal wave function is expressed in terms of normal-mode coordinates, it can be written as a product of wave functions of uncoupled harmonic oscillators. For comparison, the Einstein model also involves a crystal wave function, which is the product of wave functions for uncoupled harmonic oscillators, but each harmonic oscillator represents a particular atom and not, as for collective motion, a normal mode. The coordinate transformation that relates the displacement of atom l_u in the Lth primitive cell to real normal coordinates is given by[14]

$$\mathbf{u}_{L,l_u}=\frac{1}{\sqrt{n_s}}\sum_{\mathbf{k}}^{n_s/2}\sum_{\lambda}^{3n_u}\left[\frac{1}{\sqrt{2}}\{\epsilon^{l_u}(\mathbf{k},\lambda)\exp[2\pi i\mathbf{k}\cdot\mathbf{R}_L]+\epsilon^{l_u*}(\mathbf{k},\lambda)\exp[-2\pi i\mathbf{k}\cdot\mathbf{R}_L]\}s_{1,\mathbf{k},\lambda}+\frac{i}{\sqrt{2}}\{\epsilon^{l_u}(\mathbf{k},\lambda)\exp[2\pi i\mathbf{k}\cdot\mathbf{R}_L]-\epsilon^{l_u*}(\mathbf{k},\lambda)\times\exp[-2\pi i\mathbf{k}\cdot\mathbf{R}_L]\}s_{2,\mathbf{k},\lambda}\right], \quad (11)$$

where $\mathbf{k}$ denotes a point in the first Brillouin zone, λ denotes a mode at that $\mathbf{k}$ point, and n_s denotes the total number of atoms in the supercell. The sum over $\mathbf{k}$ ranges over half the points in the first Brillouin zone since we are using real normal-mode coordinates, denoted by s_1 and s_2. The parameter λ ranges from 1 to $3n_u$, where n_u is the number of atoms in the unit cell. We assume that our atoms are part of an infinite lattice and that the normal-mode vibrations of this lattice satisfy periodic boundary conditions defined by a supercell. The size of the supercell determines how finely the first Brillouin zone is sampled. The dispersion curves and the eigenvectors $\epsilon^{l_u}(\mathbf{k},\lambda)$ are calculated from an eigenvalue equation

$$\sum_{l'_u=1}^{n_u}\mathbf{D}^{l_ul'_u}(\mathbf{k})\cdot\epsilon^{l'_u}(\mathbf{k},\lambda)=m_A\omega_\lambda^2(\mathbf{k})\epsilon^{l_u}(\mathbf{k},\lambda), \quad (12)$$

where m_A denotes the mass of an atom (assuming a single atom type), $\omega_\lambda(\mathbf{k})$ is the angular frequency, and $\mathbf{D}^{l_ul'_u}(\mathbf{k})$ denotes the dynamical matrix. The elements of the dynamical matrix are force constants.[28] The force constants can be fitted to the dispersion curves obtained from neutron-diffraction data,[39] calculated from atomic force models, or calculated using density-functional theory.[40] To simplify the notation, we write

$$\mathbf{f}(j,\mathbf{k},\lambda,L,l_u) = \frac{i^{j-1}}{\sqrt{2n_s}}\{\epsilon^{l_u}(\mathbf{k},\lambda)\exp[2\pi i\mathbf{k}\cdot\mathbf{R}_L] + (-1)^{j-1}\epsilon^{l_u*}(\mathbf{k},\lambda)\exp[-2\pi i\mathbf{k}\cdot\mathbf{R}_L]\}, \tag{13}$$

where $j=1,2$. Hence, we can write Eq. (11) as

$$\mathbf{u}_{L,l_u} = \sum_{\mathbf{k}}^{n_s/2}\sum_{\lambda}^{3n_u}\sum_{j=1}^{2}\mathbf{f}(j,\mathbf{k},\lambda,L,l_u)s_{j,\mathbf{k},\lambda}. \tag{14}$$

To reduce the number of subscripts, we will return to using l to denote an atom, and use μ to represent the three indices $j,\lambda,\mathbf{k}$. We now write $\mathbf{u}_l \equiv \mathbf{u}_{L,l_u}$, and $s_\mu \equiv s_{j,\mathbf{k},\lambda}$.

To facilitate later calculations, we make the flat Ewald sphere approximation and write Eq. (5) as

$$\begin{aligned} W(\mathbf{q}_\perp,\mathbf{q}'_\perp) &= \frac{2\pi mK}{h^2 t_c}\int\sum_{n\neq 0} H_{0n}(\mathbf{q}_\perp - \tilde{\mathbf{K}} + K\hat{\mathbf{z}}) \\ &\quad\times H_{n0}(\tilde{\mathbf{K}} - K\hat{\mathbf{z}} - \mathbf{q}'_\perp)\delta(K-\tilde{K})d\Omega_{K'}d\tilde{K} \\ &\approx \frac{2\pi mK}{h^2 t_c}\int\sum_{n\neq 0} H_{0n}(\mathbf{q}_\perp - \tilde{\mathbf{K}} + K\hat{\mathbf{z}}) \\ &\quad\times H_{n0}(\tilde{\mathbf{K}} - K\hat{\mathbf{z}} - \mathbf{q}'_\perp)\delta(K-\tilde{K}_z)\frac{d^2\tilde{\mathbf{K}}_\perp}{\tilde{K}_z^2}d\tilde{K}_z \\ &\approx \frac{2\pi mK}{h^2 t_c}\frac{1}{K^2}\int\sum_{n\neq 0} H_{0n}(\mathbf{q}_\perp - \tilde{\mathbf{K}}_\perp) \\ &\quad\times H_{n0}(\tilde{\mathbf{K}}_\perp - \mathbf{q}'_\perp)d^2\tilde{\mathbf{K}}_\perp. \end{aligned} \tag{15}$$

In real space, the functions $H_{n0}(\mathbf{r})$ are periodic with a repeat distance equal to the length of the supercell. Hence, the Fourier components $H_{n0}(\mathbf{q})$ only take nonzero values when the argument $\mathbf{q}$ coincides with a point on the reciprocal lattice associated with the supercell. Thus, we only evaluate Eq. (15) when $\tilde{\mathbf{K}}_\perp$ lies on this phonon reciprocal lattice, and we can write the integral as a sum as follows

$$W_{\mathbf{g},\mathbf{h}} = \frac{h^2}{2\pi mt_c K}\frac{1}{A_s}\sum_{K_x,K_y}\left[\left(\frac{2m\pi}{h^2}\right)^2\sum_{n\neq 0}H_{0n}(\mathbf{h}-\mathbf{K}_s) \times H_{n0}(\mathbf{K}_s-\mathbf{g})\right]\Delta K_x\Delta K_y, \tag{16}$$

where A_s is the area of the supercell perpendicular to the zone axis and occurs as a result of the Fourier expansion. The vectors $\mathbf{K}_s$, $\mathbf{g}$, and $\mathbf{h}$ are restricted to the reciprocal lattice associated with the supercell. The term in brackets in Eq. (16) is evaluated in Appendix C. Using Eq. (C5), Eq. (16) becomes

$$\begin{aligned} W_{\mathbf{g},\mathbf{h}} &= \frac{h^2}{2\pi mA_s t_c K}\sum_{K_x,K_y}\Delta K_x\Delta K_y \\ &\quad\times\left\{\sum_l\sum_{l'}e^{-2\pi i(\mathbf{h}-\mathbf{K}_s)\cdot\mathbf{R}_{l'}}e^{-2\pi i(\mathbf{K}_s-\mathbf{g})\cdot\mathbf{R}_l}f_e(\mathbf{h}-\mathbf{K}_s)\right. \\ &\quad\times f_e(\mathbf{K}_s-\mathbf{g})[\mathcal{A}(\mathbf{h}-\mathbf{K}_s,\mathbf{K}_s-\mathbf{g},l,l') - \mathcal{B}(\mathbf{h}-\mathbf{K}_s,l) \\ &\quad\left.\times\mathcal{B}(\mathbf{K}_s-\mathbf{g},l')]\right\}. \end{aligned} \tag{17}$$

The sums over l and l' range over the atoms within a slice of the crystal as discussed in Appendix A. We have also defined

$$\mathcal{A}(\mathbf{q},\mathbf{q}',l,l') \equiv \langle\Psi_0(\mathbf{u})|e^{-2\pi i\mathbf{q}\cdot\mathbf{u}_l}e^{-2\pi i\mathbf{q}'\cdot\mathbf{u}_{l'}}|\Psi_0(\mathbf{u})\rangle, \tag{18}$$

and

$$\mathcal{B}(\mathbf{q},l) \equiv \langle\Psi_0(\mathbf{u})|e^{-2\pi i\mathbf{q}\cdot\mathbf{u}_l}|\Psi_0(\mathbf{u})\rangle. \tag{19}$$

To complete the derivation, we need to evaluate Eqs. (18) and (19) using the appropriate crystal wave functions. However, since the sample is in thermal equilibrium with the environment, there are many possible initial states. The probability of any particular initial state is determined by Bose-Einstein statistics in the canonical ensemble. Electrons that have scattered from different initial states should be summed incoherently in the detector plane. However, since this calculation cannot be performed in a reasonable time, the measurement can be modeled as though each electron scatters from a thermally averaged potential. The crystal wave function is the product of wave functions for individual modes,

$$|\Psi_0(\mathbf{s})\rangle = \prod_\mu|\Psi_0(s_\mu)\rangle. \tag{20}$$

The partition function in the canonical ensemble is the product of the partition functions of individual modes, $\mathcal{Z}=\Pi_\mu\mathcal{Z}_\mu$.[41] In Appendix D, it is shown that the thermal average of Eq. (18) is given by

$$\begin{aligned} &\frac{1}{\mathcal{Z}}\sum_n\exp\left(-\frac{E_n}{k_BT}\right)\mathcal{A}_n(\mathbf{h}-\mathbf{K}_s,\mathbf{K}_s-\mathbf{g},l,l') \\ &\quad=\prod_\mu\frac{1}{\mathcal{Z}_\mu}\sum_{n_\mu}\exp\left(-\frac{E_{n_\mu}}{k_BT}\right) \\ &\quad\times\langle\Psi_{n_\mu}(s_\mu)|e^{-2\pi i[(\mathbf{h}-\mathbf{K}_s)\cdot\mathbf{f}_{\mu,l}+(\mathbf{K}_s-\mathbf{g})\cdot\mathbf{f}_{\mu,l'}]s_\mu}|\Psi_{n_\mu}(s_\mu)\rangle \\ &\quad=\prod_\mu\exp\{-M'_\mu[(\mathbf{h}-\mathbf{K}_s)\cdot\mathbf{f}_{\mu,l}+(\mathbf{K}_s-\mathbf{g})\cdot\mathbf{f}_{\mu,l'}]^2\}, \end{aligned} \tag{21}$$

and that

$$\frac{1}{\mathcal{Z}}\sum_n \exp\left(-\frac{E_n}{k_BT}\right)\mathcal{B}_n(\mathbf{h}-\mathbf{K}_s,l)\mathcal{B}_n(\mathbf{K}_s-\mathbf{g},l')$$

$$= \prod_\mu \frac{1}{\mathcal{Z}_\mu}\sum_{n_\mu} \exp\left(-\frac{E_{n_\mu}}{k_BT}\right)$$
$$\times\langle\Psi_{n_\mu}(s_\mu)|e^{-2\pi i(\mathbf{h}-\mathbf{K}_s)\cdot\mathbf{f}_{\mu,l}s_\mu}|\Psi_{n_\mu}(s_\mu)\rangle$$
$$\times\langle\Psi_{n_\mu}(s_\mu)|e^{-2\pi i(\mathbf{K}_s-\mathbf{g})\cdot\mathbf{f}_{\mu,l'}s_\mu}|\Psi_{n_\mu}(s_\mu)\rangle$$
$$= \prod_\mu \exp\{-M'_\mu[(\mathbf{h}-\mathbf{K}_s)\cdot\mathbf{f}_{\mu,l}]^2\}$$
$$\times\exp\{-M'_\mu[(\mathbf{K}_s-\mathbf{g})\cdot\mathbf{f}_{\mu,l'}]^2\}$$
$$\times I_0[\tilde{M}_\mu|(\mathbf{h}-\mathbf{K}_s)\cdot\mathbf{f}_{\mu,l}||(\mathbf{K}_s-\mathbf{g})\cdot\mathbf{f}_{\mu,l'}|], \quad (22)$$

where

$$M'_\mu = \frac{\pi^2}{\gamma_\mu}\coth\left(\frac{\hbar\omega_\mu}{2k_BT}\right), \quad (23)$$

and

$$\tilde{M}_\mu = \frac{2\pi^2}{\gamma_\mu}\sinh^{-1}\left(\frac{\hbar\omega_\mu}{2k_BT}\right). \quad (24)$$

We have defined $\gamma_\mu = \frac{m_A\omega_\mu}{\hbar}$. The results in Eqs. (21) and (22) can be substituted back into Eq. (17) to yield

$$W_{\mathbf{h},\mathbf{g}} = \frac{h^2}{2\pi mKA_st_c}\sum_{K_x,K_y}\left\{\sum_{l'}\sum_{l} e^{-2\pi i(\mathbf{h}-\mathbf{K}_s)\cdot\mathbf{R}_{l'}}e^{-2\pi i(\mathbf{K}_s-\mathbf{g})\cdot\mathbf{R}_l}\right.$$
$$\times f_e(\mathbf{h}-\mathbf{K}_s)f_e(\mathbf{K}_s-\mathbf{g})[\exp[-(\mathbf{h}-\mathbf{K}_s)^T$$
$$\times\tilde{\mathcal{F}}(l,l')(\mathbf{K}_s-\mathbf{g})] - \exp[-(\mathbf{h}-\mathbf{K}_s)^T\tilde{\mathcal{F}}(l,l)(\mathbf{K}_s-\mathbf{g})]$$
$$\times\exp[-(\mathbf{h}-\mathbf{K}_s)^T\tilde{\mathcal{F}}(l',l')(\mathbf{K}_s-\mathbf{g})]$$
$$\left.\times\prod_\mu I_0[\tilde{M}_\mu|(\mathbf{h}-\mathbf{K}_s)\cdot\mathbf{f}_{\mu,l}||(\mathbf{K}_s-\mathbf{g})\cdot\mathbf{f}_{\mu,l'}|]\right\}\Delta K_x\Delta K_y. \quad (25)$$

The elements of the matrix $\tilde{\mathcal{F}}(l,l')$ are given by

$$\tilde{\mathcal{F}}_{i,i'}(l,l') = \sum_\mu M'_\mu f^i_{\mu,l}f^{i'}_{\mu,l'}, \quad (26)$$

where $f^i_{\mu,l}$ stands for the ith component of the vector $\mathbf{f}_{\mu,l}$. Note the sums over atoms in Eq. (25) only range over atoms in a slice perpendicular to propagation (one unit cell thick), consistent with the projected potential approximation made in Appendix A. The results of all calculations in this paper are independent of the slice chosen.

The form of the potential for phonon excitation given in Eq. (25) is significantly different from that derived in the Einstein model in Eq. (9). The potential in Eq. (25) is not parametrized by a single Debye-Waller factor but instead by the matrices $\tilde{\mathcal{F}}(l,l')$. The matrices that depend on two nonidentical atom locations contain information about the correlations between different atoms. The matrices that depend on a single atomic location, $\tilde{\mathcal{F}}(l,l)$, correspond to those defined in the anisotropic theory.[9] If the Bessel functions are ignored, the Einstein-model potential is recovered by setting $\tilde{\mathcal{F}}_{x,x}(l,l)=\tilde{\mathcal{F}}_{y,y}(l,l)=\tilde{\mathcal{F}}_{z,z}(l,l)=M_E$ and $\tilde{\mathcal{F}}_{i,i'}(l,l')=0$ otherwise.

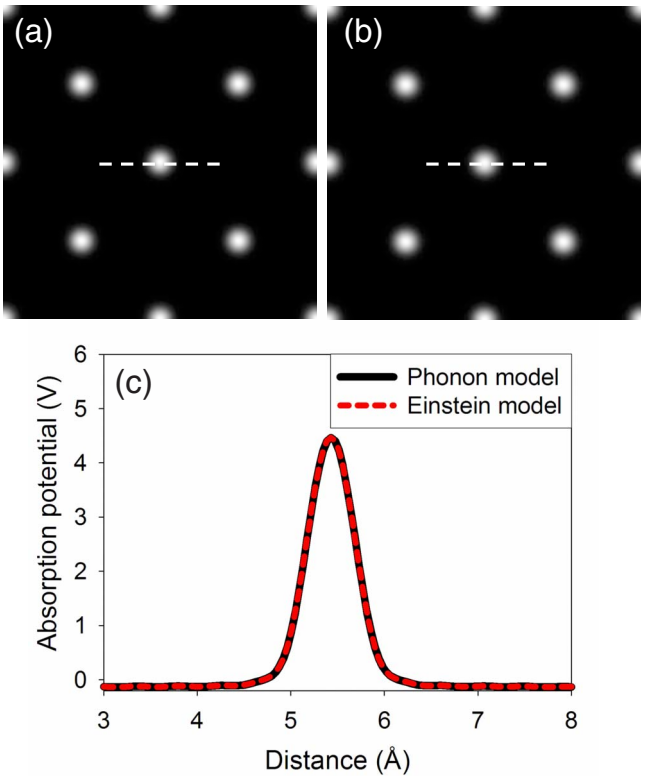

FIG. 2. (Color online) The absorption potential for a silicon crystal projected down the ⟨001⟩ axis calculated with (a) the QM-phonon model using Eq. (25) and (b) and with the Einstein model using Eq. (6). The temperature of the crystal is 293 K. The phonon calculation was performed on a supercell of size $5\times5\times5$ cubic unit cells. The potential along the dashed lines in (a) and (b) is compared in (c).

The absorption potential predicted by the Einstein model was compared with that predicted by the QM-phonon model for a silicon crystal viewed down the ⟨001⟩ axis at a temperature of 293 K. The dispersion curves were calculated using force constants for the dynamical matrix taken from Ref. 39. Note that there are some sign errors in these matrix elements. When calculating the total absorption potential, it is valid to make the local approximation in Eq. (25) by setting $W_{\mathbf{g},\mathbf{h}}\rightarrow W_{\mathbf{g}-\mathbf{h},0}$.[32] The supercell used for the QM-phonon calculation was made up of $5\times5\times5$ eight atom cubic unit cells. The Bessel functions make a negligible contribution to the phonon calculation, as they did in the Einstein-model potential, and were not included. The absorption potential predicted by the QM-phonon model is shown in Fig. 2(a) and the absorption potential predicted by the Einstein model is shown in Fig. 2(b). The line scan shown in Fig. 2(c) indicates a good agreement between the two models. As we can see in Table I, the terms in Eq. (25) that depend upon two distinct atom locations make a small contribution to the potential, indicating that correlations between different atoms do not affect the total absorption. The values of these parameters

TABLE I. Fourier components of the absorption potential calculated using Eq. (25) and the contribution from all terms containing two nonidentical atom sites ($l \neq l'$).

G	$U_{0,\mathbf{G}}$	Contribution from terms $l \neq l'$
{0 0 0}	8.43×10^{-6}	-0.02×10^{-6}
{4 4 0}	2.83×10^{-6}	0.01×10^{-7}

that depend on a single atom location, shown in Table II, confirm that for silicon at room temperature an isotropic potential described by the Debye-Waller factor is adequate. As a consequence of the QM-phonon calculation, we have a prediction for the Debye-Waller factor that agrees very well with the experimental measurement.

The agreement shown in Fig. 2 between the Einstein model and the QM-phonon model for the total absorption potential suggests that the models will agree when the local approximation is valid. If, however, the inelastic cross section is measured with a detector aperture that covers a small angular range, then key differences between the Einstein model and the QM-phonon model become evident. Consider, for example, the thermally scattered electrons that are scattered to $\mathbf{K}_s = \mathbf{0}$. We can calculate the effective potential that generates this signal by restricting the range of integration in Eq. (25) to this angle.[18] In Fig. 3(a), the effective nonlocal potential for scattering to $\mathbf{K}_s = \mathbf{0}$ for silicon is plotted as a function of x and y, for $x' = 0$ and $y' = 0$. The central peak corresponds to the contribution from the atom located at $x = 0$ and $y = 0$. All other peaks are nonlocal effects caused by correlations between this atom and the neighboring atoms. The peak heights rapidly decrease as the distance between atoms increases. If only one inelastic transition had been modeled, this decrease in peak height would not be observed and, hence, we can see how summing over all the possible phonon excitation introduces an effective "coherence length." The corresponding Einstein potential is plotted in Fig. 3(b) and as expected only shows a single peak. The heights and widths of peaks in Fig. 3(a) are determined by $\tilde{\mathcal{F}}_{i,i'}(l,l')$.

TABLE II. The parameters that appear in Eq. (25) that depend upon a single atom location, calculated for silicon at 293 K. The phonon modes were calculated on a supercell made up of $5 \times 5 \times 5$ eight atom unit cells. The experimental value of the Debye-Waller factor is included for comparison with the error given in brackets.

	(Å^2)
$\tilde{\mathcal{F}}_{x,x}(l,l)$	0.11
$\tilde{\mathcal{F}}_{y,y}(l,l)$	0.11
$\tilde{\mathcal{F}}_{z,z}(l,l)$	0.11
$\tilde{\mathcal{F}}_{x,y}(l,l)$	2.2×10^{-3}
$\tilde{\mathcal{F}}_{y,z}(l,l)$	4.2×10^{-4}
$\tilde{\mathcal{F}}_{x,z}(l,l)$	1.6×10^{-3}
Exp (Ref. 42)	0.11 (1)

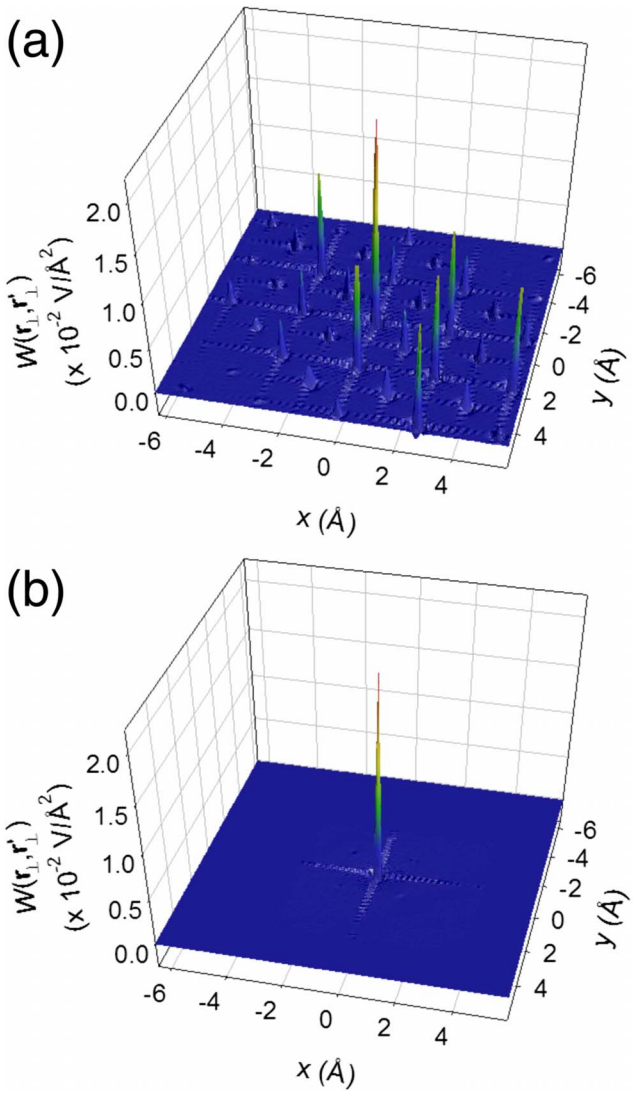

FIG. 3. (Color online) The effective absorption potential, $W(\mathbf{r}_\perp, \mathbf{r}'_\perp = \mathbf{0})$, for a point detector at $\mathbf{K}_s = \mathbf{0}$, calculated for (a) the correlated phonon model and (b) the Einstein model, for a silicon crystal viewed down the ⟨001⟩ zone axis. The temperature of the crystal is 293 K. The size of the phonon supercell was $5 \times 5 \times 5$ cubic unit cells.

In STEM, as a rule of thumb, a nonlocal potential is required when the probe-forming aperture is larger than the detector aperture.[32] However, thermally scattered electrons are typically measured in STEM at high angles with an annular detector. In most practical circumstances, the area covered by the annular detector is sufficiently large for the local approximation to be valid.

III. SCATTERED WAVES PRODUCED BY THE EXCITATION OF A PHONON

The inelastic waves generated by exciting an independently vibrating atom are different from those generated by exciting a phonon mode. The inelastic wave function produced by an inelastic-scattering event can be written as[17]

$$\psi_{\mathbf{n}}(\mathbf{r}) \approx -\frac{2\pi m}{h^2}\int \frac{e^{2\pi i k_n|\mathbf{r}-\mathbf{r}'|}}{|\mathbf{r}-\mathbf{r}'|}H_{\mathbf{n}0}(\mathbf{r}')\psi_0(\mathbf{r}')d\mathbf{r}', \quad (27)$$

where $\psi_0(\mathbf{r})$ is the elastic wave function and $\psi_{\mathbf{n}}(\mathbf{r})$ is the inelastic wave function. We have introduced the vector $\mathbf{n}=\{\ldots,n_\mu,\ldots\}$ to indicate that a crystal excitation may involve the excitation of multiple phonon modes. The transition matrix elements, $H_{\mathbf{n}0}(\mathbf{q})$, in the QM-phonon model are calculated in Appendix E and are given by

$$H_{\mathbf{n}0}(\mathbf{q}) = \sum_l e^{-2\pi i\mathbf{q}\cdot\mathbf{R}_l}\left(\frac{h^2}{2m\pi}\right)f_e(\mathbf{q})\prod_\mu \frac{1}{\sqrt{2^{n_\mu}n_\mu!}} \times(-i\sqrt{2M'_\mu})^{n_\mu}(\mathbf{f}_{\mu,l}\cdot\mathbf{q})^{n_\mu}e^{-M'_\mu(\mathbf{f}_{\mu,l}\cdot\mathbf{q})^2}. \quad (28)$$

In the QM-phonon model, the transition amplitudes take a contribution from every atom in the crystal. In contrast, the transition matrix elements calculated with the Einstein model only take a contribution from a single atom. They have been derived in Appendix F and are given by

$$H_{\mathbf{n}0}(\mathbf{q}) = (-i)^{n_1+n_2+n_3}e^{-2\pi i\mathbf{q}\cdot\mathbf{R}_l}\frac{h^2}{2m\pi}\sqrt{\frac{(2M')^{n_1+n_2+n_3}}{n_1!\,n_2!\,n_3!}} \times f_e(\mathbf{q})q_1^{n_1}q_2^{n_2}q_3^{n_3}e^{-M'q^2}. \quad (29)$$

A two-dimensional slice of an $H_{\mathbf{n}0}(\mathbf{r})$ for the QM-phonon model is shown in Fig. 4(a). The phonon model $H_{\mathbf{n}0}(\mathbf{r})$ was calculated for silicon viewed down the ⟨001⟩ zone axis and the supercell was $5\times5\times5$ eight atom unit cells. The $H_{\mathbf{n}0}(\mathbf{r})$ shown corresponds to the excitation of the mode labeled by $\mathbf{k}=(0.2,-0.2,0.6)$ Å^{-1}, $j=1$, $\omega_\mu=9.4\times10^{13}$ rad s^{-1} to the first-excited state with all other modes in the ground state. A transition potential calculated using the Einstein model is shown in Fig. 4(b). The QM-phonon model $H_{\mathbf{n}0}(\mathbf{r})$ has contributions from all atoms in the crystal, and these contributions are not the same for each atom within the supercell. In principle a measurement of inelastically scattered electrons can be simulated by calculating each of the inelastic scattered waves and propagating each to the plane of the detector, where their intensities are summed incoherently.[21] However, for phonon excitations, the large number of inelastic waves required makes this calculation impractical.

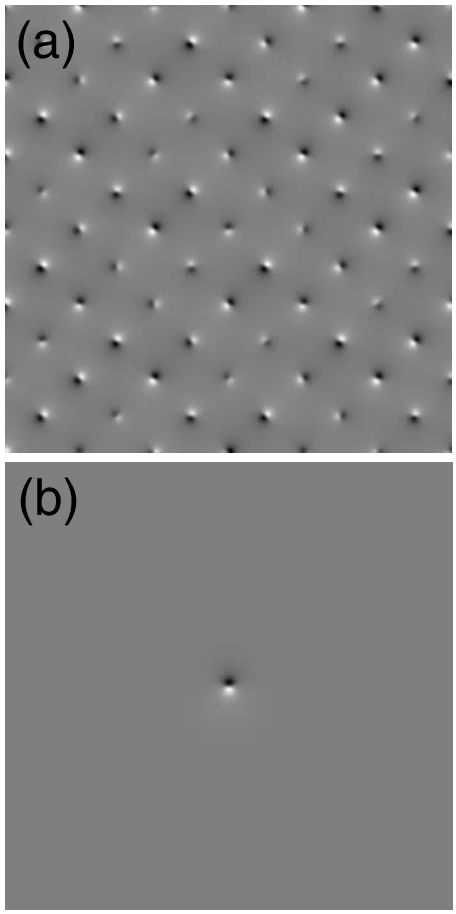

FIG. 4. The $H_{\mathbf{n}0}(\mathbf{r})$ predicted by the phonon model is shown in (a) when the mode labeled $\mathbf{k}=(0.2,-0.2,0.6)$ Å^{-1}, $j=1$, $\omega_\mu=9.4\times10^{13}$ rad s^{-1} is excited to the first-excited state. The $H_{\mathbf{n}0}(\mathbf{r})$ predicted by the Einstein model for the excitation of one harmonic oscillator to the first-excited state is shown in (b).

IV. NONLOCALITY IN THE z DIRECTION

When the nonlocal potential was projected, it was assumed that the contributions of different slices to the excitation of a particular inelastic wave do not add coherently. However, for phonon excitation this assumption is not necessarily valid. When the coherent contribution of different slices to a single inelastic wave is included in the calculation of the absorption potential, the potential becomes nonlocal in the z direction and the projected potential approximation is not made. Unlike nonlocality in the x-y plane, nonlocality in z is not affected by the detector size. It is affected by the sum over all the possible excitations, which produces a coherence length similar to that observed in Fig. 3(a). If this coherence length is small enough then the local approximation would be valid.

To gauge the level of coherence in the z direction, the quantity $W(\mathbf{r}_\perp=\mathbf{0},\ z=0,z')$ is calculated with an atom located at $\mathbf{r}_\perp=\mathbf{0}$, $z=0$. We have made a local approximation in the x and y directions. From this calculation, we obtain a simple estimate of the importance of coherence of the inelastic waves in the z direction. Figure 5 shows results for a silicon crystal viewed down the ⟨001⟩ and the ⟨110⟩ zone axes. For the ⟨001⟩ direction, the contribution to the nonlocal potential from the atom in the adjacent slice is approximately an order of magnitude lower than the contribution from the atom in the slice $z=0$. For this case, the effective coherence length is small enough to validate the use of a local potential. However, for the ⟨110⟩ direction the atom in the adjacent slice produces a peak approximately half the height of the peak over the atom at $z=0$. This could have a measurable effect on experiments that are sensitive to the thermally scattered signal. Clearly the importance of nonlocality in the z direction depends on orientation, and most likely also on crystal type. A rigorous calculation of the effect of nonlocality in z on STEM and TEM measurements is beyond the scope of this work and the subject of ongoing investigation. Nonlocality in z significantly increases the complexity of the calculation of fast electron scattering so predicting the effect on experiment is a significant challenge.

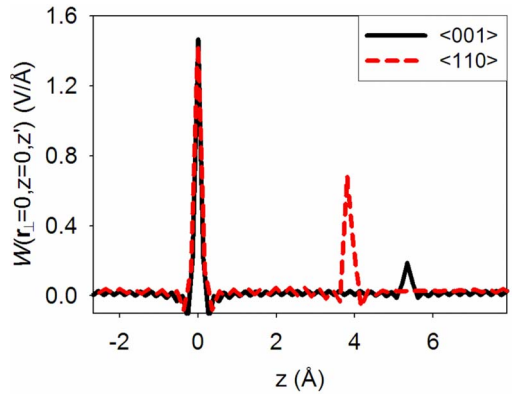

FIG. 5. (Color online) The nonlocal potential $W(\mathbf{r}_\perp=\mathbf{0}, z=0, z')$ calculated for silicon at room temperature.

V. CONCLUSION

A quantum-mechanical derivation of the absorption potential for thermal scattering based on correlated atomic motion has been presented. It has been shown that the total absorption predicted by a model with correlated atomic motion agrees with that predicted by the Einstein model based on independent atomic motion. This agreement holds when the local approximation is valid, which occurs when the detector aperture is large. Hence, we conclude that introducing correlated atomic motion will not affect the predicted contrast in simulated TEM images or in STEM HAADF images. However, the nonlocal potential associated with a small detector aperture is significantly different for the QM-phonon model as compared to the Einstein model. The inelastic scattered waves predicted by the two models are phenomenologically different since those produced by the Einstein model only take a contribution from a single atom, whereas those produced by the phonon model take a contribution from every atom in the crystal. Nonlocality in the x-y plane is shown to be important only when the detector aperture is small. Nonlocality in the z direction has been shown to occur, depending on crystal type and orientation.

APPENDIX A: PROJECTION OF THE NONLOCAL POTENTIAL

Let us expand the transition potential given by Eq. (2) as a sum of contributions from different slices

$$H_{0n}(\mathbf{r}) = \sum_\alpha \tilde{H}_{0n}^{(\alpha)}(\mathbf{r}), \tag{A1}$$

where α ranges over the number of slices in the z direction. We assume that, for convenience, each slice has the thickness of a unit cell. We write

$$\tilde{H}_{0n}^{(\alpha)}(\mathbf{r}) = \sum_{l_\alpha} \langle a_n(\boldsymbol{\tau}_n, \boldsymbol{\tau}_e) | H'_{l_\alpha}(\mathbf{r}, \boldsymbol{\tau}_n^{l_\alpha}, \boldsymbol{\tau}_e^{l_\alpha}) | a_0(\boldsymbol{\tau}_n, \boldsymbol{\tau}_e) \rangle, \tag{A2}$$

where l_α ranges only over the atoms in the slice α. The potential is projected using Eq. (4). The Fourier coefficients of the projected nonlocal potential are given by

$$W(\mathbf{q}_\perp, \mathbf{q}'_\perp) = \int e^{-2\pi i \mathbf{q}_\perp \cdot \mathbf{r}_\perp} W(\mathbf{r}_\perp, \mathbf{r}'_\perp) e^{2\pi i \mathbf{q}'_\perp \cdot \mathbf{r}'_\perp} d\mathbf{r}_\perp d\mathbf{r}'_\perp = \int e^{-2\pi i \mathbf{q}_\perp \cdot \mathbf{r}_\perp} \left[\frac{1}{t} \int_0^t \int_0^t e^{-2\pi i K z} W(\mathbf{r}, \mathbf{r}') e^{2\pi i K z'} dz dz' \right] e^{2\pi i \mathbf{q}'_\perp \cdot \mathbf{r}'_\perp} d\mathbf{r}_\perp d\mathbf{r}'_\perp$$
$$= \frac{2\pi m K}{h^2 t} \sum_{n \neq 0} \int \left[\int_0^t \int e^{-2\pi i (\mathbf{q}_\perp \cdot \mathbf{r}_\perp - \tilde{\mathbf{K}} \cdot \mathbf{r} + K z)} H_{0n}(\mathbf{r}) d\mathbf{r}_\perp dz \right] \left[\int_0^t \int e^{-2\pi i (\tilde{\mathbf{K}} \cdot \mathbf{r}' - \mathbf{q}'_\perp \cdot \mathbf{r}'_\perp - K z')} H_{n0}(\mathbf{r}') d\mathbf{r}'_\perp dz' \right] \delta(K - \tilde{K}) d\Omega_{\tilde{K}} d\tilde{K}. \tag{A3}$$

Defining the thickness of a unit cell to be t_c and substituting Eq. (A1) into Eq. (A3), we find

$$W(\mathbf{q}_\perp, \mathbf{q}'_\perp) = \frac{2\pi m K}{h^2 t} \sum_{n \neq 0} \int \left[\int e^{-2\pi i (\mathbf{q}_\perp \cdot \mathbf{r}_\perp - \tilde{\mathbf{K}} \cdot \mathbf{r} + K z)} \sum_\alpha \int_{z_\alpha}^{z_\alpha + t_c} \tilde{H}_{0n}^{(\alpha)}(\mathbf{r}) dz d\mathbf{r}_\perp \right]$$
$$\times \left[\int e^{-2\pi i (\tilde{\mathbf{K}} \cdot \mathbf{r}' - \mathbf{q}'_\perp \cdot \mathbf{r}'_\perp - K z')} \sum_{\alpha'} \int_{z_{\alpha'}}^{z_{\alpha'} + t_c} \tilde{H}_{n0}^{(\alpha')}(\mathbf{r}') dz' d\mathbf{r}'_\perp \right] \delta(K - \tilde{K}) d\Omega_{\tilde{K}} d\tilde{K}. \tag{A4}$$

The range of the integration over dz has been restricted to the width of a slice since it is assumed that $\tilde{H}_{0n}^{(\alpha)}(\mathbf{r})$ is localized within this range. In order to have a potential that is local in the z direction, we must have incoherence in the z direction, which we enforce by setting $\alpha = \alpha'$. Note that in the Einstein model this is rigorously justified. In the QM-phonon model, the sum over all the excitations n may introduce an effective coherence length. If this coherence length is less than the width of a unit cell, the sum over the all the terms where $\alpha \neq \alpha'$ equals zero, validating this step. Making this approximation we have

$$W(\mathbf{q}_\perp, \mathbf{q}'_\perp) = \frac{2\pi m K}{h^2 t} \sum_\alpha \sum_{n \neq 0} \int \left[\int \int_{z_\alpha}^{z_\alpha + t_c} e^{-2\pi i (\mathbf{q}_\perp \cdot \mathbf{r}_\perp - \tilde{\mathbf{K}} \cdot \mathbf{r} + K z)} \tilde{H}_{0n}^{(\alpha)}(\mathbf{r}) dz d\mathbf{r}_\perp \right] \left[\int \int_{z_\alpha}^{z_\alpha + t_c} e^{-2\pi i (\tilde{\mathbf{K}} \cdot \mathbf{r}' - \mathbf{q}'_\perp \cdot \mathbf{r}'_\perp - K z')} \tilde{H}_{n0}^{(\alpha)}(\mathbf{r}') dz' d\mathbf{r}'_\perp \right]$$
$$\times \delta(K - \tilde{K}) d\Omega_{\tilde{K}} d\tilde{K}. \tag{A5}$$

Now we assume that, having summed over the excited states n, the nonlocal potential for each slice will be the same. Hence, we only have to calculate the potential for a single slice and multiply by the number of slices N. Since the thickness of a slice is $t_c=t/N$, we have

$$W(\mathbf{q}_\perp,\mathbf{q}'_\perp)=\frac{2\pi mK}{h^2t_c}\sum_{n\neq 0}\int\left[\int\int_0^{t_c}e^{-2\pi i(\mathbf{q}_\perp\cdot\mathbf{r}_\perp-\tilde{\mathbf{K}}\cdot\mathbf{r}+Kz)}\tilde{H}_{0n}(\mathbf{r})dzd\mathbf{r}_\perp\right]\left[\int\int_0^{t_c}e^{-2\pi i(\tilde{\mathbf{K}}\cdot\mathbf{r}'-\mathbf{q}'_\perp\cdot\mathbf{r}'_\perp-Kz')}\tilde{H}_{n0}(\mathbf{r}')dz'd\mathbf{r}'_\perp\right]$$
$$\times\delta(K-\tilde{K})d\Omega_{\tilde{K}}d\tilde{K}. \tag{A6}$$

Since the function $\tilde{H}_{0n}(\mathbf{r})$ is localized within the range of $0-t_c$, the limits of the integration over dz and dz' can be taken to infinity and we have

$$W(\mathbf{q}_\perp,\mathbf{q}'_\perp)=\frac{2\pi mK}{h^2t_c}\sum_{n\neq 0}\int\tilde{H}_{0n}(\mathbf{q}_\perp-\tilde{\mathbf{K}}+K\hat{\mathbf{z}})$$
$$\times\tilde{H}_{n0}(\tilde{\mathbf{K}}-\mathbf{q}'_\perp-K\hat{\mathbf{z}})\delta(K-\tilde{K})d\Omega_{\tilde{K}}d\tilde{K}. \tag{A7}$$

In the main text, we will drop the tilde and write $H_{0n}(\mathbf{q})$. It is implicit that the sum over atoms ranges over one slice in the supercell perpendicular to propagation.

APPENDIX B: NONLOCAL ABSORPTION POTENTIAL FOR THE EINSTEIN MODEL

In a model where the atoms vibrate independently, we assume the many-body crystal wave function can be written as a product of wave functions for each atom:

$$|a_0(\boldsymbol{\tau}_n,\boldsymbol{\tau}_e)\rangle=\prod_l|a_0(\boldsymbol{\tau}_n^l,\boldsymbol{\tau}_e^l)\rangle. \tag{B1}$$

We can evaluate the terms in Eq. (5) that depend upon n as follows

$$\sum_{n\neq 0}H_{0n}(\mathbf{q}_\perp-\mathbf{K}')H_{n0}(\mathbf{K}'-\mathbf{q}'_\perp)$$
$$=\sum_l\sum_{l'}\langle a_0(\boldsymbol{\tau}_n,\boldsymbol{\tau}_e)|H'_l\left[\sum_{n\neq 0}|a_n(\boldsymbol{\tau}_n,\boldsymbol{\tau}_e)\rangle\langle a_n(\boldsymbol{\tau}_n,\boldsymbol{\tau}_e)|\right]$$
$$\times H'_{l'}|a_0(\boldsymbol{\tau}_n,\boldsymbol{\tau}_e)\rangle=\sum_l\sum_{l'}\langle a_0(\boldsymbol{\tau}_n,\boldsymbol{\tau}_e)|H'_l[1-|a_0(\boldsymbol{\tau}_n,\boldsymbol{\tau}_e)\rangle$$
$$\times\langle a_0(\boldsymbol{\tau}_n,\boldsymbol{\tau}_e)|]H'_{l'}|a_0(\boldsymbol{\tau}_n,\boldsymbol{\tau}_e)\rangle$$
$$=\sum_l\sum_{l'}\langle a_0(\boldsymbol{\tau}_n,\boldsymbol{\tau}_e)|H'_lH'_{l'}|a_0(\boldsymbol{\tau}_n,\boldsymbol{\tau}_e)\rangle$$
$$-\sum_l\sum_{l'}\langle a_0(\boldsymbol{\tau}_n,\boldsymbol{\tau}_e)|H'_l|a_0(\boldsymbol{\tau}_n,\boldsymbol{\tau}_e)\rangle$$
$$\times\langle a_0(\boldsymbol{\tau}_n,\boldsymbol{\tau}_e)|H'_{l'}|a_0(\boldsymbol{\tau}_n,\boldsymbol{\tau}_e)\rangle, \tag{B2}$$

where we have written $H'_l=H'_l(\mathbf{q}_\perp-\mathbf{K}',\boldsymbol{\tau}_n^l,\boldsymbol{\tau}_e^l)$ and $H'_{l'}=H'_{l'}(\mathbf{K}'-\mathbf{q}'_\perp,\boldsymbol{\tau}_n^{l'},\boldsymbol{\tau}_e^{l'})$. Using Eq. (B1) and the orthogonality of the crystal eigenstates, we find that

$$\langle a_0(\boldsymbol{\tau}_n,\boldsymbol{\tau}_e)|H'_l|a_0(\boldsymbol{\tau}_n,\boldsymbol{\tau}_e)\rangle=\langle a_0(\boldsymbol{\tau}_n^l,\boldsymbol{\tau}_e^l)|H'_l|a_0(\boldsymbol{\tau}_n^l,\boldsymbol{\tau}_e^l)\rangle, \tag{B3}$$

and that

$$\langle a_0(\boldsymbol{\tau}_n,\boldsymbol{\tau}_e)|H'_lH'_{l'}|a_0(\boldsymbol{\tau}_n,\boldsymbol{\tau}_e)\rangle=\begin{cases}\langle a_0(\boldsymbol{\tau}_n^l,\boldsymbol{\tau}_e^l)|H'_lH'_l|a_0(\boldsymbol{\tau}_n^l,\boldsymbol{\tau}_e^l)\rangle, & \text{if } l=l'\\ \langle a_0(\boldsymbol{\tau}_n^l,\boldsymbol{\tau}_e^l)|H'_l|a_0(\boldsymbol{\tau}_n^l,\boldsymbol{\tau}_e^l)\rangle\langle a_0(\boldsymbol{\tau}_n^{l'},\boldsymbol{\tau}_e^{l'})|H'_{l'}|a_0(\boldsymbol{\tau}_n^{l'},\boldsymbol{\tau}_e^{l'})\rangle, & \text{if } l\neq l'.\end{cases} \tag{B4}$$

When we substitute Eqs. (B3) and (B4) into the last line of Eq. (B2), there is a cancellation for all the terms where $l\neq l'$, and we are left with

$$\sum_{n\neq 0}H_{0n}(\mathbf{q}_\perp-\mathbf{K}')H_{n0}(\mathbf{K}'-\mathbf{q}'_\perp)=\sum_l[\langle a_0(\boldsymbol{\tau}_n^l,\boldsymbol{\tau}_e^l)|H'_lH'_l|a_0(\boldsymbol{\tau}_n^l,\boldsymbol{\tau}_e^l)\rangle-\langle a_0(\boldsymbol{\tau}_n^l,\boldsymbol{\tau}_e^l)|H'_l|a_0(\boldsymbol{\tau}_n^l,\boldsymbol{\tau}_e^l)\rangle\langle a_0(\boldsymbol{\tau}_n^l,\boldsymbol{\tau}_e^l)|H'_l|a_0(\tau_n^l,\boldsymbol{\tau}_e^l)\rangle]. \tag{B5}$$

Equation (B5) can be evaluated with harmonic-oscillator wave functions in the same manner as Ref. 13 to obtain

$$W(\mathbf{q}_\perp,\mathbf{q}'_\perp)=\frac{Kh^2}{2\pi mV_c}\left[\sum_l e^{-2\pi i(\mathbf{q}_\perp-\mathbf{q}'_\perp)\cdot\mathbf{R}_l}\right]\int f_e(\mathbf{q}_\perp-\mathbf{K}')f_e(\mathbf{K}'-\mathbf{q}'_\perp)\{e^{-M_E(\mathbf{q}_\perp-\mathbf{q}'_\perp)^2}-e^{-M_E(\mathbf{q}_\perp-\mathbf{K}')^2}e^{-M_E(\mathbf{K}'-\mathbf{q}'_\perp)^2}$$
$$\times I_0[\tilde{M}|(\mathbf{q}_\perp-\mathbf{K}')_x||(\mathbf{K}'-\mathbf{q}'_\perp)_x|]I_0[\tilde{M}|(\mathbf{q}_\perp-\mathbf{K}')_y||(\mathbf{K}'-\mathbf{q}'_\perp)_y|]I_0[\tilde{M}|(\mathbf{q}_\perp-\mathbf{K}')_z||(\mathbf{K}'-\mathbf{q}'_\perp)_z|]\}d\Omega_{K'}. \tag{B6}$$

APPENDIX C: PRELIMINARY STEPS IN THE DERIVATION OF THE ABSORPTION POTENTIAL FOR PHONON EXCITATION

The atomic coordinates of an atom in a crystal can be written as the sum of an equilibrium location and a displacement, $\boldsymbol{\tau}_n^l = \mathbf{R}_l + \mathbf{u}_l$. Similarly, the electronic coordinates can be rewritten relative to the nuclear coordinate, $\boldsymbol{\tau}_e^{l,i} = \boldsymbol{\tau}_e'^{l,i} + \mathbf{R}_l + \mathbf{u}_l$. Using these definitions, Eq. (3) becomes

$$H_{n0}(\mathbf{r}) = \langle a_n(\mathbf{u}, \boldsymbol{\tau}_e')| \sum_l \left[\frac{Z_N e^2}{4\pi\epsilon_0 |\mathbf{r} - (\mathbf{R}_l + \mathbf{u}_l)|} - \sum_{i=1}^{N} \frac{e^2}{4\pi\epsilon_0 |\mathbf{r} - (\boldsymbol{\tau}_e'^{l,i} + \mathbf{R}_l + \mathbf{u}_l)|} \right] |a_0(\mathbf{u}, \boldsymbol{\tau}_e')\rangle. \tag{C1}$$

Using the standard identity

$$\int \frac{1}{|\mathbf{r} - \mathbf{r}'|} e^{2\pi i \mathbf{q}\cdot\mathbf{r}} d\mathbf{r} = \frac{1}{\pi |\mathbf{q}|^2} e^{2\pi i \mathbf{q}\cdot\mathbf{r}'}, \tag{C2}$$

we may substitute Eq. (C2) into Eq. (C1) to obtain

$$H_{n0}(\mathbf{q}) = \sum_l e^{-2\pi i \mathbf{q}\cdot\mathbf{R}_l} \langle a_n(\mathbf{u}, \boldsymbol{\tau}_e')| \left[\frac{Z_N e^2}{4\pi^2 \epsilon_0 |\mathbf{q}|^2} e^{-2\pi i \mathbf{q}\cdot\mathbf{u}_l} - \sum_{i=1}^{N} \frac{e^2}{4\pi^2 \epsilon_0 |\mathbf{q}|^2} e^{-2\pi i \mathbf{q}\cdot(\boldsymbol{\tau}_e'^{l,i} + \mathbf{u}_l)} \right] |a_0(\mathbf{u}, \boldsymbol{\tau}_e')\rangle. \tag{C3}$$

Assuming that the nuclear and electronic motions are decoupled, we write $|a_n(\mathbf{u}, \boldsymbol{\tau}_e')\rangle = |\Psi_n(\mathbf{u})\rangle |a_n'(\boldsymbol{\tau}_e')\rangle$ and then integrate over the electronic coordinates. This gives

$$\frac{2m\pi}{h^2} H_{n0}(\mathbf{q}) = \sum_l e^{-2\pi i \mathbf{q}\cdot\mathbf{R}_l} f_e(\mathbf{q}) \langle \Psi_n(\mathbf{u})| e^{-2\pi i \mathbf{q}\cdot\mathbf{u}_l} |\Psi_0(\mathbf{u})\rangle, \tag{C4}$$

where $f_e(\mathbf{q})$ is the electron-scattering factor. Using Eq. (C4) and repeating the steps in Eq. (B2), the term in brackets in Eq. (16) can be evaluated

$$\left(\frac{2m\pi}{h^2}\right)^2 \sum_{n\neq 0} H_{0n}(\mathbf{q} - \mathbf{K}_s) H_{n0}(\mathbf{K}_s - \mathbf{q}') = \sum_l \sum_{l'} e^{-2\pi i (\mathbf{q} - \mathbf{K}_s)\cdot\mathbf{R}_{l'}} e^{-2\pi i (\mathbf{K}_s - \mathbf{q}')\cdot\mathbf{R}_l} f_e(\mathbf{q} - \mathbf{K}_s) f_e(\mathbf{K}_s - \mathbf{q}') \times [\mathcal{A}(\mathbf{q} - \mathbf{K}_s, \mathbf{K}_s - \mathbf{q}', l, l') - \mathcal{B}(\mathbf{q} - \mathbf{K}_s, l)\mathcal{B}(\mathbf{K}_s - \mathbf{q}', l')], \tag{C5}$$

where

$$\mathcal{A}(\mathbf{q}, \mathbf{q}', l, l') \equiv \langle \Psi_0(\mathbf{u})| e^{-2\pi i \mathbf{q}\cdot\mathbf{u}_l} e^{-2\pi i \mathbf{q}'\cdot\mathbf{u}_{l'}} |\Psi_0(\mathbf{u})\rangle, \tag{C6}$$

and

$$\mathcal{B}(\mathbf{q}, l) \equiv \langle \Psi_0(\mathbf{u})| e^{-2\pi i \mathbf{q}\cdot\mathbf{u}_l} |\Psi_0(\mathbf{u})\rangle. \tag{C7}$$

APPENDIX D: THERMAL AVERAGE OF THE POTENTIAL

To evaluate Eq. (21) we define

$$E_{n_\mu} = \hbar\omega_\mu \left(n_\mu + \frac{1}{2}\right), \tag{D1}$$

$$\mathcal{Z}_\mu = \sum_{n_\mu} \exp\left(-\frac{E_{n_\mu}}{k_B T}\right) = \frac{\exp\left(-\frac{\hbar\omega_\mu}{2k_B T}\right)}{1 - \exp\left(-\frac{\hbar\omega_\mu}{k_B T}\right)}, \tag{D2}$$

$$\psi_{n_\mu}(s_\mu) = N_{n_\mu} e^{-(1/2)\gamma_\mu s_\mu^2} \mathrm{H}_{n_\mu}(\sqrt{\gamma_\mu} s_\mu), \tag{D3}$$

$$\gamma_\mu = \frac{m_A \omega_\mu}{\hbar}, \tag{D4}$$

$$\mathrm{H}_{n_\mu}(s_\mu) = (-1)^{n_\mu} e^{s_\mu^2} \frac{d^{n_\mu}}{ds_\mu^{n_\mu}} e^{-s_\mu^2}, \tag{D5}$$

$$N_{n_\mu} = \left(\frac{\gamma_\mu}{\pi}\right)^{1/4} \frac{1}{\sqrt{2^{n_\mu} n_\mu!}}. \tag{D6}$$

For convenience define $z_\mu \equiv \exp(-\frac{\hbar\omega_\mu}{k_B T})$, where we note $z_\mu < 1$ and that $\mathcal{Z}_\mu = \frac{\sqrt{z_\mu}}{1 - z_\mu}$. Using Eqs. (D3) and (D6) we can write

$$\begin{aligned} &\langle \Psi_{n_\mu}(s_\mu)| e^{-2\pi i q s_\mu} |\Psi_{n_\mu}(s_\mu)\rangle \\ &= N_{n_\mu}^2 \int_{-\infty}^{\infty} e^{-2\pi i q s_\mu} e^{-\gamma_\mu s_\mu^2} \mathrm{H}_{n_\mu}(\sqrt{\gamma_\mu} s_\mu) \mathrm{H}_{n_\mu}(\sqrt{\gamma_\mu} s_\mu) ds_\mu \\ &= \frac{1}{\sqrt{\pi} 2^{n_\mu} n_\mu!} \int_{-\infty}^{\infty} \exp\left[-2\pi i \frac{q}{\sqrt{\gamma_\mu}} x\right] e^{-x^2} \mathrm{H}_{n_\mu}(x) \mathrm{H}_{n_\mu}(x) dx, \end{aligned} \tag{D7}$$

where we have performed a change in variables given by $x = \sqrt{\gamma_\mu} s_\mu$. The integral may be evaluated via a standard result[43]

$$\int_{-\infty}^{\infty} \frac{dx e^{-x^2} e^{i\beta x} \mathrm{H}_n(x) \mathrm{H}_m(x)}{\sqrt{\pi} 2^{n/2} 2^{m/2} \sqrt{n!\, m!}} = \sqrt{\frac{2^m m!}{2^n n!}} (i\beta)^{n-m} L_m^{n-m}\left(\frac{\beta^2}{2}\right) e^{-\beta^2/4}, \tag{D8}$$

in which the $L_m^\alpha(z)$ are the associated Laguerre polynomials and the values of m, n are restricted to the integers $0, 1, 2, 3\ldots$.[44] Thus, the amplitude for a particular mode appearing in Eq. (21) is

$$\langle \Psi_{n_\mu}(s_\mu)|e^{-2\pi i[\mathbf{q}\cdot\mathbf{f}_{\mu,l}+\mathbf{q}'\cdot\mathbf{f}_{\mu,l'}]s_\mu}|\Psi_n(s_\mu)\rangle = \exp\left(-\frac{\pi^2}{\gamma_\mu}[\mathbf{q}\cdot\mathbf{f}_{\mu,l}+\mathbf{q}'\cdot\mathbf{f}_{\mu,l'}]^2\right)L_{n_\mu}^0\left(\frac{2\pi^2}{\gamma_\mu}[\mathbf{q}\cdot\mathbf{f}_{\mu,l}+\mathbf{q}'\cdot\mathbf{f}_{\mu,l'}]^2\right). \tag{D9}$$

Taking the thermal average of Eq. (D9) we find

$$\begin{aligned}
&\frac{1}{\mathcal{Z}_\mu}\sum_{n_\mu}\exp\left(-\frac{E_{n_\mu}}{k_BT}\right)\exp\left(-\frac{\pi^2}{\gamma_\mu}[\mathbf{q}\cdot\mathbf{f}_{\mu,l}+\mathbf{q}'\cdot\mathbf{f}_{\mu,l'}]^2\right)L_{n_\mu}^0\left(\frac{2\pi^2}{\gamma_\mu}[\mathbf{q}\cdot\mathbf{f}_{\mu,l}+\mathbf{q}'\cdot\mathbf{f}_{\mu,l'}]^2\right)\\
&\quad=(1-z_\mu)\exp\left(-\frac{\pi^2}{\gamma_\mu}[\mathbf{q}\cdot\mathbf{f}_{\mu,l}+\mathbf{q}'\cdot\mathbf{f}_{\mu,l'}]^2\right)\sum_{n_\mu}z_\mu^{n_\mu}L_{n_\mu}^0\left(\frac{2\pi^2}{\gamma_\mu}[\mathbf{q}\cdot\mathbf{f}_{\mu,l}+\mathbf{q}'\cdot\mathbf{f}_{\mu,l'}]^2\right)\\
&\quad=\frac{1-z_\mu}{1-z_\mu}\exp\left(-\frac{\pi^2}{\gamma_\mu}[\mathbf{q}\cdot\mathbf{f}_{\mu,l}+\mathbf{q}'\cdot\mathbf{f}_{\mu,l'}]^2\right)\exp\left(-\frac{2\pi^2}{\gamma_\mu}[\mathbf{q}\cdot\mathbf{f}_{\mu,l}+\mathbf{q}'\cdot\mathbf{f}_{\mu,l'}]^2\frac{z_\mu}{1-z_\mu}\right)\\
&\quad=\exp\left[-\frac{\pi^2}{\gamma_\mu}[\mathbf{q}\cdot\mathbf{f}_{\mu,l}+\mathbf{q}'\cdot\mathbf{f}_{\mu,l'}]^2\left(\frac{2z_\mu}{1-z_\mu}+1\right)\right]=\exp\left(-\frac{\pi^2}{\gamma_\mu}\frac{1+z_\mu}{1-z_\mu}[\mathbf{q}\cdot\mathbf{f}_{\mu,l}+\mathbf{q}'\cdot\mathbf{f}_{\mu,l'}]^2\right)\\
&\quad=\exp\left[-\pi^2\frac{\hbar}{m\omega_\mu}\coth\left(\frac{\hbar\omega_\mu}{2k_BT}\right)[\mathbf{q}\cdot\mathbf{f}_{\mu,l}+\mathbf{q}'\cdot\mathbf{f}_{\mu,l'}]^2\right]=\exp(-M'_\mu[\mathbf{q}\cdot\mathbf{f}_{\mu,l}+\mathbf{q}'\cdot\mathbf{f}_{\mu,l'}]^2),
\end{aligned} \tag{D10}$$

where M'_μ is given by

$$M'_\mu=\pi^2\frac{\hbar}{m_A\omega_\mu}\coth\left(\frac{\hbar\omega_\mu}{2k_BT}\right). \tag{D11}$$

The step from the second line to the third line in Eq. (D10) involved the standard result[44]

$$\sum_{n=0}^{\infty}L_n^\alpha(x)z^n=\frac{1}{(1-z)^{\alpha+1}}\exp\left(-\frac{xz}{1-z}\right),\quad |z|<1. \tag{D12}$$

Hence, substituting Eq. (D10) into Eq. (21) we obtain

$$\begin{aligned}
&\frac{1}{\mathcal{Z}}\sum_n\exp\left(-\frac{E_n}{k_BT}\right)\mathcal{A}_n(\mathbf{h}-\mathbf{K}_s,\mathbf{K}_s-\mathbf{g},l,l')\\
&\quad=\prod_\mu\frac{1}{\mathcal{Z}_\mu}\sum_{n_\mu}\exp\left(-\frac{E_{n_\mu}}{k_BT}\right)\\
&\quad\times\langle\Psi_{n_\mu}(s_\mu)|e^{-2\pi i[(\mathbf{h}-\mathbf{K}_s)\cdot\mathbf{f}_{\mu,l}+(\mathbf{K}_s-\mathbf{g})\cdot\mathbf{f}_{\mu,l'}]s_\mu}|\Psi_{n_\mu}(s_\mu)\rangle\\
&\quad=\prod_\mu\exp\{-M'_\mu[(\mathbf{h}-\mathbf{K}_s)\cdot\mathbf{f}_{\mu,l}+(\mathbf{K}_s-\mathbf{g})\cdot\mathbf{f}_{\mu,l'}]^2\}.
\end{aligned} \tag{D13}$$

To evaluate Eq. (22), we start by using Eq. (D8) to write

$$\begin{aligned}
&\frac{1}{\mathcal{Z}_\mu}\sum_{n_\mu}\exp\left(-\frac{E_{n_\mu}}{k_BT}\right)\mathcal{B}_n(\mathbf{q},l)\mathcal{B}_n(\mathbf{q}',l')=\frac{1-z_\mu}{\sqrt{z_\mu}}\sum_{n_\mu}\sqrt{z_\mu}z_\mu^{n_\mu}\exp\left[-\frac{\pi^2}{\gamma_\mu}(\mathbf{q}\cdot\mathbf{f}_{\mu,l})^2\right]L_{n_\mu}^0\left[\frac{2\pi^2}{\gamma_\mu}(\mathbf{q}\cdot\mathbf{f}_{\mu,l})^2\right]\\
&\quad\times\exp\left[-\frac{\pi^2}{\gamma_\mu}(\mathbf{q}'\cdot\mathbf{f}_{\mu,l'})^2\right]L_{n_\mu}^0\left[\frac{2\pi^2}{\gamma_\mu}(\mathbf{q}'\cdot\mathbf{f}_{\mu,l'})^2\right]=(1-z_\mu)\exp\left[-\frac{\pi^2}{\gamma_\mu}(\mathbf{q}\cdot\mathbf{f}_{\mu,l})^2\right]\\
&\quad\times\exp\left[-\frac{\pi^2}{\gamma}(\mathbf{q}'\cdot\mathbf{f}_{\mu,l'})^2\right]\sum_{n_\mu}z_\mu^{n_\mu}L_{n_\mu}^0\left[\frac{2\pi^2}{\gamma_\mu}(\mathbf{q}\cdot\mathbf{f}_{\mu,l})^2\right]L_{n_\mu}^0\left[\frac{2\pi^2}{\gamma_\mu}(\mathbf{q}'\cdot\mathbf{f}_{\mu,l'})^2\right]=(1-z_\mu)\exp\left[-\frac{\pi^2}{\gamma_\mu}(\mathbf{q}\cdot\mathbf{f}_{\mu,l})^2\right]\\
&\quad\times\exp\left(-\frac{\pi^2}{\gamma_\mu}q_j'^2\right)\frac{1}{1-z_\mu}\exp\left[-\frac{\pi^2}{\gamma_\mu}(\mathbf{q}\cdot\mathbf{f}_{\mu,l})^2\frac{2z_\mu}{1-z_\mu}\right]\exp\left[-\frac{\pi^2}{\gamma_\mu}(\mathbf{q}'\cdot\mathbf{f}_{\mu,l'})^2\frac{2z_\mu}{1-z_\mu}\right]I_0\left[\frac{2\sqrt{z_\mu}}{1-z_\mu}\sqrt{\frac{2\pi^2}{\gamma_\mu}(\mathbf{q}\cdot\mathbf{f}_{\mu,l})^2\frac{2\pi^2}{\gamma_\mu}(\mathbf{q}'\cdot\mathbf{f}_{\mu,l'})^2}\right]\\
&\quad=\exp\left[-\frac{\pi^2}{\gamma_\mu}(\mathbf{q}\cdot\mathbf{f}_{\mu,l})^2\frac{1+z_\mu}{1-z_\mu}\right]\exp\left[-\frac{\pi^2}{\gamma}(\mathbf{q}'\cdot\mathbf{f}_{\mu,l'})^2\frac{1+z_\mu}{1-z_\mu}\right]I_0\left[\frac{2\sqrt{z_\mu}}{1-z_\mu}\frac{2\pi^2}{\gamma_\mu}|(\mathbf{q}\cdot\mathbf{f}_{\mu,l})||(\mathbf{q}'\cdot\mathbf{f}_{\mu,l'})|\right]\\
&\quad=\exp[-M'_\mu(\mathbf{q}\cdot\mathbf{f}_{\mu,l})^2]\exp[-M'_\mu(\mathbf{q}'\cdot\mathbf{f}_{\mu,l'})^2]I_0\left[4\pi^2/\gamma_\mu 1/\frac{1}{\sqrt{z}}-\sqrt{z}|(\mathbf{q}\cdot\mathbf{f}_{\mu,l})||(\mathbf{q}'\cdot\mathbf{f}_{\mu,l'})|\right]\\
&\quad=\exp[-M'_\mu(\mathbf{q}\cdot\mathbf{f}_{\mu,l})^2]\exp[-M'_\mu(\mathbf{q}'\cdot\mathbf{f}_{\mu,l'})^2]I_0\left[2\pi^2/\gamma_\mu|(\mathbf{q}\cdot\mathbf{f}_{\mu,l})||(\mathbf{q}'\cdot\mathbf{f}_{\mu,l'})|/\sinh\left(\frac{\hbar\omega_\mu}{2k_BT}\right)\right].
\end{aligned} \tag{D14}$$

In the step from the second line to the third line, the sum was performed using the standard result[44]

$$\sum_{n=0}^{\infty} \frac{n!}{\Gamma(1+m+n)} z^n L_n^m(x) L_n^m(y) = \frac{\exp\left[-(x+y)\frac{z}{1-z}\right]}{1-z} I_m\left(2\sqrt{xy}\frac{\sqrt{z}}{1-z}\right) \frac{1}{(xyz)^{m/2}}, \quad |z|<1. \tag{D15}$$

Hence, using Eqs. (D14) and (24) we can evaluate Eq. (22) as follows

$$\begin{aligned}
&\frac{1}{\mathcal{Z}}\sum_n \exp\left(-\frac{E_n}{k_B T}\right)\mathcal{B}_n(\mathbf{h}-\mathbf{K}_s,l)\mathcal{B}_n(\mathbf{K}_s-\mathbf{g},l') \\
&= \prod_\mu \frac{1}{\mathcal{Z}_\mu}\sum_{n_\mu} \exp\left(-\frac{E_{n_\mu}}{k_B T}\right) \\
&\times \langle \Psi_{n_\mu}(s_\mu)| e^{-2\pi i(\mathbf{h}-\mathbf{K}_s)\cdot \mathbf{f}_{\mu,l} s_\mu} |\Psi_{n_\mu}(s_\mu)\rangle \\
&\times \langle \Psi_{n_\mu}(s_\mu)| e^{-2\pi i(\mathbf{K}_s-\mathbf{g})\cdot \mathbf{f}_{\mu,l'} s_\mu} |\Psi_{n_\mu}(s_\mu)\rangle \\
&= \prod_\mu \exp\{-M'_\mu[(\mathbf{h}-\mathbf{K}_s)\cdot \mathbf{f}_{\mu,l}]^2\} \\
&\times \exp\{-M'_\mu[(\mathbf{K}_s-\mathbf{g})\cdot \mathbf{f}_{\mu,l'}]^2\} \\
&\times I_0[\tilde{M}_\mu|(\mathbf{h}-\mathbf{K}_s)\cdot \mathbf{f}_{\mu,l}||(\mathbf{K}_s-\mathbf{g})\cdot \mathbf{f}_{\mu,l'}|],
\end{aligned} \tag{D16}$$

where

$$\tilde{M}_\mu = \frac{2\pi^2}{\gamma_\mu}\sinh^{-1}\left(\frac{\hbar\omega_\mu}{2k_B T}\right). \tag{D17}$$

APPENDIX E: DERIVATION OF THE H_{n0} FOR THE QM-PHONON MODEL

In normal-mode coordinates the many-body wave function can be factorized in terms of normal-mode wave functions, as given by Eq. (20). Hence, Eq. (C4) becomes

$$H_{\mathbf{n}0}(\mathbf{q}) = \sum_l \left(\frac{h^2}{2m\pi}\right) f_e(\mathbf{q}) e^{-2\pi i \mathbf{q}\cdot\mathbf{R}_l} \times \prod_\mu \langle \Psi_n(s_\mu)| e^{-2\pi i(\mathbf{q}\cdot\mathbf{f}_{\mu,l})s_\mu} |\Psi_0(s_\mu)\rangle. \tag{E1}$$

The crystal wave functions are given by Eq. (D3). Using the standard result in Eq. (D8) it is easy to show that

$$\langle \Psi_{n_\mu}(s_\mu)| e^{-2\pi i(\mathbf{q}\cdot\mathbf{f}_{\mu,l})s_\mu} |\Psi_0(s_\mu)\rangle = \frac{1}{\sqrt{2^{n_\mu} n_\mu!}}(-i\sqrt{2M'_\mu})^{n_\mu} \times (\mathbf{q}\cdot\mathbf{f}_{\mu,l})^{n_\mu} e^{-M'_\mu(\mathbf{q}\cdot\mathbf{f}_{\mu,l})^2}. \tag{E2}$$

Substituting Eq. (E2) into Eq. (E1) gives

$$H_{\mathbf{n}0}(\mathbf{q}) = \sum_l e^{-2\pi i \mathbf{q}\cdot\mathbf{R}_l}\left(\frac{h^2}{2m\pi}\right) f_e(\mathbf{q}) \prod_\mu \frac{1}{\sqrt{2^{n_\mu} n_\mu!}}(-i\sqrt{2M'_\mu})^{n_\mu} \times (\mathbf{q}\cdot\mathbf{f}_{\mu,l})^{n_\mu} e^{-M'_\mu(\mathbf{q}\cdot\mathbf{f}_{\mu,l})^2}. \tag{E3}$$

APPENDIX F: DERIVATION OF THE H_{n0} FOR THE EINSTEIN MODEL

In the Einstein model, each nucleus is located in a harmonic potential well. Assuming an isotropic potential, the atomic wave function for the nuclear coordinates factorizes into a product of wave functions for three orthogonal directions, each of which has the standard harmonic-oscillator wave-function form

$$|\Psi_0(\mathbf{u})\rangle = |\Psi_0(u_1)\rangle|\Psi_0(u_2)\rangle|\Psi_0(u_3)\rangle, \tag{F1}$$

where $\mathbf{u}$ denotes the displacement of the atom from its equilibrium position. Hence, Eq. (C4) becomes

$$H_{\mathbf{n}0}(\mathbf{q}) = \left(\frac{h^2}{2m\pi}\right) f_e(\mathbf{q}) e^{-2\pi i \mathbf{q}\cdot\mathbf{R}_l} \prod_i \langle \Psi_n(u_i)| e^{-2\pi i q_i u_i} |\Psi_0(u_i)\rangle. \tag{F2}$$

The crystal wave functions $|\Psi_0(u_i)\rangle$ are harmonic-oscillator wave functions and hence using the same steps as in Appendix E we find

$$H_{\mathbf{n}0}(\mathbf{q}) = (-i)^{n_1+n_2+n_3} e^{-2\pi i \mathbf{q}\cdot\mathbf{R}_l} \frac{h^2}{2m\pi} \times \sqrt{\frac{(2M')^{n_1+n_2+n_3}}{n_1!\, n_2!\, n_3!}} f_e(\mathbf{q}) q_1^{n_1} q_2^{n_2} q_3^{n_3} e^{-M' q^2}. \tag{F3}$$

[1] C. R. Hall and P. B. Hirsch, Proc. R. Soc. London, Ser. A **286**, 158 (1965).
[2] M. J. Whelan, J. Appl. Phys. **36**, 2103 (1965).
[3] J. M. Cowley and A. P. Pogany, Acta Crystallogr., Sect. A: Cryst. Phys., Diffr., Theor. Gen. Crystallogr. **24**, 109 (1968).
[4] D. M. Bird and Q. A. King, Acta Crystallogr., Sect. A: Found. Crystallogr. **46**, 202 (1990).
[5] R. F. Loane, P. Xu, and J. Silcox, Acta Crystallogr., Sect. A: Found. Crystallogr. **47**, 267 (1991).
[6] S. L. Dudarev, L.-M. Peng, and M. J. Whelan, Phys. Rev. B **48**, 13408 (1993).
[7] Z. L. Wang, *Elastic and Inelastic Scattering in Electron Diffraction and Imaging* (Plenum Press, New York, 1995).
[8] C. Dinges, A. Berger, and H. Rose, Ultramicroscopy **60**, 49 (1995).
[9] L.-M. Peng, Acta Crystallogr., Sect. A: Found. Crystallogr. **53**, 663 (1997).
[10] H. X. Gao and L.-M. Peng, Acta Crystallogr., Sect. A: Found.

Crystallogr. **55**, 926 (1999).
[11] C. B. Boothroyd, J. Microsc. **190**, 99 (1998).
[12] R. A. Herring, Ultramicroscopy **106**, 960 (2006).
[13] A. L. Weickenmeier and H. Kohl, Acta Crystallogr., Sect. A: Found. Crystallogr. **54**, 283 (1998).
[14] D. A. Muller, B. Edwards, E. J. Kirkland, and J. Silcox, Ultramicroscopy **86**, 371 (2001).
[15] J. M. LeBeau, S. D. Findlay, L. J. Allen, and S. Stemmer, Phys. Rev. Lett. **100**, 206101 (2008).
[16] C. J. Humphreys, Rep. Prog. Phys. **42**, 1825 (1979).
[17] H. Yoshioka, J. Phys. Soc. Jpn. **12**, 618 (1957).
[18] L. J. Allen and T. W. Josefsson, Phys. Rev. B **52**, 3184 (1995).
[19] E. J. Kirkland, *Advanced Computing in Electron Microscopy* (Plenum Press, New York, 1998).
[20] Z. H. Levine, Phys. Rev. B **77**, 125314 (2008).
[21] C. Dwyer, S. D. Findlay, and L. J. Allen, Phys. Rev. B **77**, 184107 (2008).
[22] L. Reimer, *Transmission Electron Microscopy* (Springer-Verlag, New York, 1984).
[23] M. J. Hÿtch and W. M. Stobbs, Ultramicroscopy **53**, 191 (1994).
[24] A. Howie, Ultramicroscopy **98**, 73 (2004).
[25] S. J. Pennycook and D. E. Jesson, Ultramicroscopy **37**, 14 (1991).
[26] D. Van Dyck, Ultramicroscopy **109**, 677 (2009).
[27] P. Rez, C. J. Humphreys, and M. J. Whelan, Philos. Mag. **35**, 81 (1977).
[28] M. Born and K. Huang, *Dynamical Theory of Crystal Lattices* (Clarendon Press, Oxford, 1956).
[29] C. Fanidis, D. Van Dyck, and J. Van Landuyt, Ultramicroscopy **48**, 133 (1993).
[30] C. Dwyer, Ultramicroscopy **104**, 141 (2005).
[31] S. D. Findlay, L. J. Allen, M. P. Oxley, and C. J. Rossouw, Ultramicroscopy **96**, 65 (2003).
[32] S. D. Findlay, M. P. Oxley, and L. J. Allen, Microsc. Microanal. **14**, 48 (2008).
[33] H. Ibach, Phys. Rev. Lett. **24**, 1416 (1970).
[34] H. Ibach and D. Bruchmann, Phys. Rev. Lett. **44**, 36 (1980).
[35] A. A. Lucas and M. Sunjic, Phys. Rev. Lett. **26**, 229 (1971).
[36] D. E. Jesson and S. J. Pennycook, Proc. R. Soc. London, Ser. A **449**, 273 (1995).
[37] W. Coene and D. Van Dyck, Ultramicroscopy **33**, 261 (1990).
[38] B. T. M. Willis and A. W. Pryor, *Thermal Vibrations in Crystallography* (Cambridge University Press, Cambridge, 1975).
[39] W. Jian, Z. Kaiming, and X. Xide, Solid State Commun. **86**, 731 (1993).
[40] S. Baroni, S. de Gironcoli, and A. D. Corso, Rev. Mod. Phys. **73**, 515 (2001).
[41] D. J. Amit and Y. Verben, *Statistical Physics* (World Scientific, Singapore, 1995).
[42] N. M. Butt and J. Bashir, Acta Crystallogr., Sect. A: Found. Crystallogr. **44**, 396 (1988).
[43] R. A. Bonham and G. G. B. de Souza, J. Chem. Phys. **79**, 134 (1983).
[44] H. Buchholz, *The Confluent Hypergeometric Function* (Springer-Verlag New York Inc., New York, 1969).